Journal of Molecular Liquids 413 (2024) 125815

Contents lists available at ScienceDirect

Journal of Molecular Liquids

journal homepage: www.elsevier.com/locate/molliq

Surface-modified silica nanoparticles for enhanced oil recovery in sandstone cores

Louey Tliba [a], Farad Sagala [d], Afif Hethnawi [d], Paul W.J. Glover [c], Robert Menzel [b], Ali Hassanpour [a,*]

[a] School of Chemical and Process Engineering, Faculty of Engineering and Physical Science, University of Leeds, Leeds LS2 9JT, UK
[b] School of Chemistry, Faculty of Engineering and Physical Science, University of Leeds, Leeds LS2 9JT, UK
[c] School of Earth and Environment, University of Leeds, Leeds LS2 9JT, UK
[d] Department of Chemical and Petroleum Engineering, University of Calgary, Calgary, Alberta T2N1N4, Canada

ARTICLE INFO

Keywords:
SiO_2 nanoparticles
Grafting
Contact angle
Spontaneous imbibition
Wettability alteration

ABSTRACT

Enhanced Oil Recovery (EOR) techniques traditionally employ chemical flooding; however, recent integration of nanoparticles (NPs) with water flooding has demonstrated promising enhancements in oil recovery. Silica (SiO_2) NPs have been widely used in this regard, however, the primary challenge is their tendency to aggregate in solution due to their ultra-small size and large surface area, which can inhibit their effectiveness in EOR applications. To address this, we modified the surface of commercially sourced SiO_2 NPs using two different agents: polyethylenimine (PEI) for polymer coating and Triethoxy(octyl)silane (TOS) for covalent surface functionalisation, without any binders or preliminary coatings. The modified NPs (TOS-NPs and PEI-NPs) were characterized using techniques such as SEM, TEM, FTIR, TGA, BET and DLS. Their efficacy in EOR was evaluated within sandstone cores through measurements of contact angle, interfacial tension (IFT), and spontaneous imbibition tests. Results indicated that the surface modifications substantially improved the stability of the SiO_2 NPs. Specifically, TOS-NPs effectively altered the wettability of sandstone cores from strongly oil-wet (27°) to strongly water-wet (165°), in contrast to PEI-NPs (16°) and unmodified SiO_2 NPs (94°). IFT measurements revealed a 78 % reduction with PEI-NPs, compared to only 5 % with TOS-NPs. In spontaneous imbibition tests, TOS-NPs achieved the highest oil recovery, approximately 64.9 % without noticeable core plugging, compared to 53.0 % for the unmodified NPs and 9.8 % by PEI-NPs. These results, alongside the contact angle measurements, confirm that for the sandstone wettability alteration of the rock could be the major contributing mechanism for EOR using TOS-NPs.

1. Introduction

Conventionally, only about one-third of the petroleum in known reservoirs can be recovered using current technology via primary and secondary recovery methods. These methods are selected based on a variety of economic and technological considerations [1]. In principle, the primary recovery method utilises the inherent pressure of the reservoir to extract oil [2]. Following pressure depletion, secondary recovery methods, such as water and/or gas injection, are employed to drive the oil [3]. The effectiveness of these methods is limited to hydrocarbons that can be naturally moved or displaced towards the surface, exhibiting limited sweep and displacement efficiency. Thus, petroleum engineering researchers have focused on developing tertiary recovery technologies, such as chemical enhanced oil recovery (cEOR), aiming to improve overall oil recovery rates [3,4]. These cEOR techniques employ surfactants, polymers, and/or alkalis to enhance both microscopic displacement and/or macroscopic sweeping efficiencies [5–7]. There are challenges associated with cEOR. For instance, polymer

Abbreviations: EOR, Enhanced Oil Recovery; NPs, Nanoparticles; SiO_2, Silica nanoparticle; PEI, Polyethylenimine; DW, Deionised water; TEM, Transmission Electron Microscopy; TGA, Thermo-gravimetric analysis; ZP, Zeta Potential; BET, Brunauer-Emmet-Teller; TOS, Triethoxy(octyl)silane; IFT, Interfacial tension; BS, Brine solution; LSW, Low salinity water; cEOR, Chemical enhanced oil recovery; FTIR, Fourier Transform Infrared spectroscopy; SEM, Scanning Electron Microscope; DLS, Dynamic Light Scattering; SI, Supporting Information.

* Corresponding author.
E-mail address: a.hassanpour@leeds.ac.uk (A. Hassanpour).

https://doi.org/10.1016/j.molliq.2024.125815
Received 24 March 2024; Received in revised form 9 August 2024; Accepted 19 August 2024
Available online 22 August 2024

flooding is limited by harsh conditions such as high salinity and temperature, necessitating evaluations of polymer thermal stability to prevent equipment clogging and chemical precipitation [8]. Alkaline flooding (AF) also faces challenges such as precipitation and scaling [5,9]. These challenges highlight the growing need to develop new, cost-effective, efficient, and environmentally friendly EOR technologies [10].

Over the past two decades, the application of nanoparticles (NPs) as EOR agents has attracted the attention of researchers to address the limitations and challenges caused by the traditional methods [11,12]. Nanocarriers in the form of nanofluids (i.e., liquid suspensions of different kinds of NPs, such as metals, oxides, carbides, carbon nanotubes, etc.) have shown promise in improving oil recovery [13–15]. These nanofluids are known to enhance oil recovery through reported mechanisms such as structural disjoining pressure, reduction of oil–water interfacial tension (IFT), and alteration of rock surface wettability, etc. [16–18]. The disjoining pressure mechanism, in particular, effectively moves oil through the self-wedge film formed by NPs in the confined three-phase regions of oil, solid, and nanofluid [19,20]. This movement is driven by the electrostatic repulsion and Brownian motion of the NPs [21]. As their size decreases, both the charge density and electrostatic repulsion increase, thus improving their EOR efficiency [21]. Additionally, these NPs can form a film layer at the oil–water interface, further reducing the IFT [15,22]. Research by Adel et al. [23] demonstrated that both silicon dioxide (SiO_2) and aluminum oxide (Al_2O_3) nanofluids significantly reduce IFT under ambient conditions, with SiO_2 nanofluid showing particularly low IFT values. Moreover, studies have shown that NPs can alter the wettability of rocks from oil-wet to more water-wet conditions, a key mechanism in EOR [24,25]. For instance, Ju and Fan [26] found that hydrophilic SiO_2 NPs changed the wettability of oil-wet sandstones, as confirmed by TEM-images showing NPs adsorption on rock surfaces. Further research by Hendraningrat et al. [27] revealed that SiO_2 NPs can significantly modify rock wettability from strongly oil-wet to strongly water-wet. Additionally, Lucky et al. [28] explored the effect of SiO_2 NPs on oil recovery, examined different parameters including particle size, permeability, and rock wettability. They discovered that smaller NPs effectively decreased the contact angle between oil and rock, improving oil recovery. The best results were observed in systems with intermediate wettability, attributed to the wettability changes caused by the adsorption of SiO_2 NPs on rock surfaces.

However, NPs on their own tend to agglomerate under aqueous conditions to minimize their high surface energies, which limits their effectiveness in EOR applications [18,29,30]. Consequently, different studies have reported some surface modifications or grafting with diverse polymers and chemical agents to facilitate the dispersing of these nanomaterials [31]. SiO_2 NPs is a dominant substance in sandstone reservoirs and is one of the most abundant non-toxic materials with low production costs compared to other NPs, making it the preferred agent for EOR [32,33]. Numerous research studies have focused on the application of SiO_2 NPs in EOR, highlighting their potential to improve oil recovery efficiencies [28,34,35]. However, the effectiveness of SiO_2 NPs as EOR agents is often limited by their tendency to agglomerate in aqueous conditions due to the high surface energy and van der Waals forces between particles, which may result in rock pore blockage [29,31]. Surface modification of SiO_2 NPs, such as by silanisation or polymer coating, can significantly improve their stability in suspensions, preventing aggregation and ensuring their effective distribution in the rock formations, thus avoiding pore blockage [12,36]. For instance, Alberto Bila, et al.[37], investigated the effect of polymer-coated SiO_2 NPs (AEROSIL® particles) on oil recovery in neutral-wet Berea. Their study included two-phase core flooding tests under ambient conditions: secondary using water followed by nanofluid flooding, and tertiary recovery beginning with nanofluid injecting followed by water flooding. They explored several mechanisms of NPs −EOR, such as wettability alteration of the rock surface, IFT reduction, and the log-jamming effect. The results indicated that using polymer-coated SiO_2 NPs in secondary recovery had improved oil recovery by altering the wettability of Berea from neutral to water–wet, identifying wettability alteration as the primary mechanism for EOR. However, IFT reduction did not significantly impact oil recovery. In another study, Haruna et al. [38] modified SiO_2 NPs with (3-amino propyl) triethoxysilane to introduce positively charged functional groups onto the surfaces of the NPs. This modification was intended to enhance interactions with the negatively charged polyacrylamide (PAM) polymer, significantly improving the dispersion stability of the SiO_2 NPs. They conducted core flooding test on Berea sandstone cores with both unmodified and PAM-functionalised SiO_2 NPs. The modified NPs increased oil recovery by approximately 10 % more than unmodified SiO_2 NPs. Furthermore, Caili et al. [39] enhanced the surface properties and stability of SiO_2 NPs using a two-step modification process. Initially, vinyl trimethoxy silane was used to bond with the SiO_2 NPs hydroxyl groups, introducing reactive vinyl groups. This was followed by applying 2-mercaptobenzimidazole as a stabilizing agent, which bonded to the vinyl-modified surface via the (−SH) group. This improved the stability and dispersity of NPs for EOR applications. In their study, a spontaneous imbibition test was conducted on sandstone cores immersed in three liquids: 0.1 wt% SiO_2 nanofluids, pH10 alkaline water, and NaCl solution. Their results showed that after 12 days, the SiO_2 nanofluid recovered approximately 38 % of the oil, compared to only 12 and 6 % recovered with alkaline water and NaCl solution, respectively. The primary mechanism for the EOR was identified as the alteration of core surface wettability from oil-wet to water-wet, demonstrated by an increase in the oil contact angle from 42° to 122° after introducing the nanofluid, compared to minimal increase after using other liquids, where the contact angle was measured to the less dense phase (oil). Despite these changes, the IFT of oil/nanofluid remained the same as that of oil/water and oil/NaCl, at 24 mN/m. In a study by Ganesh et al. a functional SiO_2 nanofluid was developed by synergistically combining positively charged Ludox CL silica NPs (modified SiO_2 NPs) with an anionic Aerosol-OT (AOT) surfactant in low-salinity water (LSW) [25]. By varying the concentrations of AOT and NPs, they prepared different nanofluid and conducted a spontaneous imbibition test at an average reservoir temperature of about 60 °C. The nanofluid with 37.5 ppm AOT and 1.5 wt% NPs achieved the highest oil recovery, approximately 48 % of the original oil in place (OIIP), compared to only around 10 % recovery for both LSW and deionized water (DW). This nanofluid demonstrated improved stability and notably altered the wettability of Berea sandstone from oil-wet (with a contact angle of 119° for DW) to strongly water-wet (with contact angle of 15° for the nanofluid), where the contact angle was measured to the high dense phase (water). This wettability alteration of the rock surface was accompanied by 52 % reduction in IFT compared to DW.

The methods and procedures mentioned for stabilizing SiO_2 NPs are complex, requiring high temperature, multiple steps, and initial grafting with chemical handles. As a results, these processes can be costly and energy intensive. Therefore, it would be of significant interest to develop more cost-effective treatment and grafting methods that can be integrate with other conventional EOR technologies.

While previous studies often rely on multi-step procedures for NPs modifications of in-house synthesized silica NPs or silica NPs in liquid dispersions, in this work we focus on simple one-step modification process of commercially available SiO_2 powders under relatively mild conditions, enhancing energy efficiency using low temperatures and pressure. This study conducts a comparative investigation into the modification of SiO_2 NPs with two specific agents, polyethyleneimine (PEI) and Triethoxy(octyl)silane (TOS). Both systems are examined under identical conditions, facilitating a direct comparison between these two distinct functionalization approaches: non-covalent coating with a hydrophilic polymer and covalent boding with a hydrophobic, molecular capping agent. While PEI and TOS have previously been used to functionalise pyroxene NPs (resulting in EOR of approximately 25 % with PEI [40], and between 28 % [40] to 35 % with TOS [41]), this work

represents the first instance of their application with commercially sourced SiO_2 NPs.

Diverse characterisation techniques, such as transmission electron microscopy (TEM), scanning electron microscope (SEM), fourier-transform infrared spectroscopy (FTIR), thermogravimetric analysis (TGA), Brunauer–Emmett–Teller (BET), Zetasizer-Nano series, and dynamic light scattering (DLS) were conducted to confirm the surface properties, functionality, stability, and morphology of the prepared SiO_2 NPs. Subsequently, these nanomaterials were dispersed in selected LSW to evaluate their effectiveness for EOR applications, using contact angle and IFT measurements. Furthermore, displacement tests using spontaneous imbibition method were employed to assess the effectiveness of the newly developed nanofluid in enhancing oil recovery from saturated Berea sandstone cores.

2. Materials and experimental methods

2.1. Materials

SiO_2 NPs (10–20 nm particle size, with 99.5 % purity), Branched amino-based polymer (polyethylenimine) with MW Mn ~ 60,000 (PEI), silane-based agent (triethoxy(octyl)silane) (TOS) with 97 % purity (TOS), and cyclohexane (99 % purity) were all purchased from Sigma-Aldrich and used as received. Magnesium chloride ($MgCl_2$ 99 %), calcium chloride ($CaCl_2$ 99 %), sodium chloride (NaCl 99 %), and potassium chloride (KCl 99 %) were obtained from VWR and were also used with no further purification. DW was used as the dispersant fluid for the prepared NPs. The pH was measured using a digital pH meter after calibration. Stranded nitric acid (0.1 N), and sodium hydroxide were used to adjust the pH. Algerian crude oil was used as the source of oil in this work, with a viscosity of 71 cP at 20 °C and 13 cP at 60 °C, an API gravity of 24.6, and an asphaltene content of approximately 0.25 %. Sandstone core plugs with a porosity ranging from 20 % to 22 % were utilized.

2.2. Nanoparticle modification

The functionalisation of the NPs was adapted from the protocol reported by Afif et al.[42] for producing stable NPs dispersions. Given the objectives of our staudy, we found it necessary to modify certain aspects of this protocol to optimize the properties of the NPs for the EOR application.

In this study, commercial SiO_2 NPs were modified with PEI and TOS to evaluate their stability and applicability as Enhanced Oil Recovery agent (EOR). For the PEI modification, initially 500 mg of SiO_2 NPs were dispersed in 70 ml of DW using an Ultraturax disperser at 8000 rpm for 10 min to (temporarily) break up most of the larger SiO_2 into smaller clusters, followed by stirring at 300 rpm for 30 min at room temperature (Solution 1).

Subsequently, 0.5 g of PEI was added to 30 ml of DW, and the resulting solution (desiganted as Solution 2) was stirred at 250 rpm for 1 h. The pH of Solution 2 was adjusted with hydrochloric acid, followed by an additional stirring over a period of 10 min. Solution 1 was then gradually added to Solution 2 using a pipette over a duration of 12 min. The mixture was further stirred at 250 rpm for 3 h at ambient temperature. Following a 48 h settling period, the samples were separated, washed, and subsequently subjected to two different freezing protocols: overnight storage in the freezer at(−20 °C) or a 10 min immersion in a liquid nitrogen bath at (−196 °C). After freezing, the samples were placed in a freeze dryer for 48 h to sublimate frozen water. The resultant NPs, referred to as PEI-NPs, were synthesized using a consistent protocol with modifications in the pH of Solution 2 to assess the impact of pH on PEI loading onto SiO_2 NPs. This adjustment aimed to identify the optimal pH value that maximises PEI loading, therby enhancing the functionality of the PEI-NPs.

The second modification approach was based on grafting TOS onto the surface of commercial SiO_2 NPs. In brief, 500 mg of SiO_2 NPs were dispersed in 80 ml of cyclohexane using an ultraturex at 8000 rpm followed by sonication for 1 h in an ice cooled sonication bath to (temporarily) break up most of the larger SiO_2 into smaller clusters. The temperature during sonication was maintained at approximately 22 °C. Cyclohexane was specifically chosen due to its effectiveness in dissolving TOS, facilitating the functionalisation process [41]. Then, 2.5 g of TOS was gradually added to the dispersed solution under stirring at 300 rpm. Three different samples were prepared by varying the stirring time to 2, 3, and 24 h. Afterwards, the prepared solution was centrifuged at 5000 rpm for 15 min, and the supernatant was decanted. The precipitate was recovered and washed with methanol, and then placed in a vacuum oven at 60 °C for 3 h. The resulting sample was denoted as TOS-NPs.

2.3. Fluid formulations

2.3.1. Nanofluid formulation

Different nanofluids were prepared, including unmodified and modified SiO_2 NPs. Initially the samples were investigated for the stability of the prepared NPs, where 0.005 wt% of each nanoparticle was dispersed in DW then ultrasonicated for 15 min using an ultrasonic bath. This concentration was selected based on previous reported studies [28,41,43,44]. Subsequently, another batch was prepared by dispersing an optimised concentration (approximately 0.005 wt%) of each prepared material into the selected LSW. The resulting nanofluids was ready for different analyses.

2.3.2. Brine solution

Four different salts ($MgCl_2$, $CaCl_2$, NaCl, and KCl) were used to formulate various brine solutions to assess the efficacy of the prepared NPs as EOR agents under saline conditions [45]. Typical range of formation brine salinity in oil reservoirs is from 1000 to 400,000 ppm [46,47]. In this study, the brine solution (BS) was prepared in seven different forms applicable to the lower range of formation brine salinities, as summarized in the table below (Table 1), when deionized water was used as the base fluid.

2.3.3. Asphaltene quantification

The amount of asphaltene in the oil samples was determined following a standard procedure [48]. In a beaker of 500 ml, 10 mL of oil was mixed with 400 mL of n-heptane. The mixture was boiled for 35 min to speed up the precipitation process before allowing it to cool and settle down over night. The mixture was filtered several times through filter paper (8 μm particle retention) in a vacuum filtration. The amount of asphaltene was calculated using the weight difference between the filter before and after filtration. Figure S1 (all Figures denoted with S are in the supplementary information) shows the filter papers after the filtration of crude oil, and the asphaltene content was approximately 0.25 %.

2.4. Characterisation of nanoparticle and nanofluids

2.4.1. Brunauer-Emmet-Teller (BET)

To determine the effect of anchoring PEI or TOS agent on the surface area of the virgin SiO_2 NPs, the BET-Gas adsorption technique (BET, Micomeritics Tristar 3000) was used in this study. This technique is commonly applied to measure the surface area and porosity of the

Table 1
Composition of different BS.

BS sample	A (wt %)	B (wt %)	C (wt %)	D (wt %)	E (wt %)	F (wt %)	G (wt %)	H (wt %)
NaCl	0	0.05	0.1	0.2	1	2	2	2
KCl	0	0	0	0	0	0	0.2	0.2
$CaCl_2$	0	0	0	0	0	0	0.2	0.4
$MgCl_2$	0	0	0	0	0	0	0.1	0.2

powders in the micro-and mesoporous range. All the prepared NPs were used in their solid form. Before the BET analysis, the prepared samples were firstly degassed, inside a degasser unit (Micromeritics Flow Prep 060 sample Degas System), with a nitrogen gas flow and concurrently heated to 423 K overnight to remove any water or other species from the surface and pores of the materials and ensure that they are clean. Following N_2 degassing, all samples were weighted to determine weight inputs for the software calculations. Finally, the samples were submitted to the adsorption–desorption of nitrogen at 77 K to produce the adsorption–desorption isotherms.

2.4.2. Fourier transform infrared spectroscopy (FTIR)

This provides precise qualitative analyses of the functional groups that react in a sample. In this study, FT-ir Nicolet iS10 from Thermo-Fisher Scientific was used to identify the main functional groups and the molecular bonds that existed in the SiO_2 NPs before and after anchoring PEI or TOS agent. The samples were prepared by mixing 6 mg of each sample with 500 mg of KBr and then mounted on the DRIFTS holder. Each sample was measured in a transmission mode at a spectrum range between 400 and 4000 cm^{-1}. With a resolution of 2 cm^{-1} and the spectrum was the average of 128 scans.

2.4.3. Thermo-gravimetric analysis (TGA)

The loaded amount of PEI or TOS at the surface of the SiO_2 NPs was estimated using TGA analysis (TGA – Mettler Toledo TGA/DSC1). Approximately 10 mg of solid form sample was placed in a 70 μL alumina crucible and weighed before being placed in the TGA/DSC1 sample holder. All TGA measurements were carried out at a ramped temperature range of 30 °C–900 °C, at a rate of 10 °C/min, and under a continuous airflow rate of 50 ml/min.

2.4.4. Zetasizer and dynamic light scattering (DLS)

Zeta potential (ZP) analyses were performed using the Malvern Zetasizer Nano ZS/ZSP instrument (MRK654-01) to study the stability of the differently prepared nanofluids at room and high temperatures and under different saline conditions. This technique was also used to test the sand/brine interface for different prepared BS. All ZP measurements were performed on a zetasizer software with the Smoluchowaski approximation option for aqueous systems at 60 s equilibration time and ambient temperatures or high temperature in autoprocessing mode. For sand/brine ZP measurements, around 0.5 g of sand (ground from the same sandstone sample) was mixed with different prepared fluids at room temperature. Then for all other tests, a small amount of prepared nanofluid was filled with a syringe into disposable folded capillary cells of 1 ml size. The instrument was set up to collect three data points for each sample and report an average arithmetic result for each analysis [49]. The measurements were repeated three times for reproducibility, and the average ZP values were reported.

The hydrodynamic size distributions of the prepared nanoparticles were determined utilizing a dynamic light scattering (DLS) using the Malvern Zetasizer Nano ZS/ZSP instrument (MRK654-01).

2.4.5. Cold field emission scanning electron microscope (CFE-SEM)

In this study, the SEM imaging was carried out using a cold field emission scanning electron microscope (Hitachi SU8230 CFE-SEM). This technique provides the morphology, size, and structure of the nano-materials before and after surface modification. A small quantity of each sample (~0.6 mg) was dispersed in 5 mL of DW and sonicated for approximately 5 min to ensure that the samples were suspended. A single drop was then placed on the SEM stub and allowed to dry. Subsequently, an acceleration voltage of 2 kV for SEM was used to image the particles' surfaces at various length scales (500 nm,200 nm, 100 nm, and 50 nm).

2.4.6. Transmission electron microscopy (TEM)

This technique investigated particle morphology, size distribution, and structure before and after functionalisation with PEI or TOS agents. TEM measurements were performed using the FEI Titan Themis Cubed operated at 300 kV and fitted with a Monochromator. A small quantity of each sample was suspended *via* ultrasonication in 5 mL DW solvent before a single drop was placed on a carbon-coated copper grid and allowed to dry.

TEM experiments were conducted using an accerlarting volatage of 20 kV and that images were collected on a Gatan Oneview 16 Megapixel CMOS digital camera with a screen current of 2nA, fitted with the Super-X EDX system with four windowless detectors. Spectra were collected in TEM mode with an exposure time of 10 s using Velox software.

2.5. Enhanced oil recovery (EOR) measurements

2.5.1. Contact angle and IFT measurements

The contact angle measurements were used to obtain a quantitative assessment of the wettability of the core plugs before and after treatment with nanofluids using Biolinc Scientific Attention Theta Flex optical tensiometer. Polished sandstone substrates were cut to fit the cube chamber. Then they were aged in oil for approximately one week at 70 °C and atmospheric pressure to change their initial wettability. Afterward the substrates were left to dry in an oven for six hours at 60 °C [41].

The wettability of the sandstone substrate was evaluated first with an oil drop before and after ageing in oil. Afterward, cores aged in oil were immersed in different prepared fluids/nanofluids. This process occurred over a period of two days and at a temperature of 60ºC. Subsequently, each substrate was dried in a 55 °C oven for two hours [41]. Contact angle measurements involving sandstone substrate, oil drop, brine or nanofluid was analysed to determine the effect of the nanofluid on wettability change. The contact angle was measured towards the less dense phase (oil) over a specific period of time.

On the other hand, to determine the effect of different nanofluids on the IFT between oil and aqueous phases at ambient conditions, the IFT was carried out using a pendant drop method with a tensiometer (Biolin Scientific Attension Theta Flex optical tensiometer). For each measurement, a drop of crude oil was formed at the tip of a hooked needle inside a chamber filled with different fluids/nanofluids. Then, IFT was determined between the oil droplet and the liquid inside the chamber for a given time interval (2000 s).

2.5.2. Preparation and characterisation of sandstone cores

Berea sandstone core plug with 3.8 cm diameter and 30 cm length was cut into different smaller core plugs with the rough length of 3.8 cm. The porosity of these cores was measured at room temperature using helium gas expansion. The permeability measurements were Klinkenberg-corrected and utilised nitrogen as the process gas. Table 2 (a) presents the petrophysical properties of the core samples in this study. Additionally, a core sample was cut into three different slices, as shown in Fig. S19, and each part was crushed into small slices then pulverized to obtain a very fine powder using a ball mill Spex 8000 M. A Thermo Scientific iCAP7400 ICP-OES was employed for digested rock samples, which were analysed undiluted. Yttrium (371.030 nm) and lutetium (261.542 nm) at a concentration of 1 mg L^{-1} was added to all standards and samples as internal standards. Direct calibration using 2 % of HNO_3 as a diluent was employed for the analysis. Table 2(b) displays the ICP analyses for the digested core samples. FTIR analysis was also conducted on the milled sand powder, as illustrated in Fig S2. To conduct solid/brine ZP measurements, a small piece of the core with a 3.8 cm diameter and length of 1.3 cm was crushed. The crushed core was subsequently transformed into a fine powder, using the Retsch Vibratory Disc Mill RS 200, for measurements with the Zetasizer analyses.

2.5.3. Spontaneous imbibition test

The spontaneous imbibition tests are static techniques that can be used to evaluate the performance of prepared nanofluids for EOR. This

Table 2a
The petrophysical details for cores used for all experiments.

Core samples	Length (cm)	Diameter (cm)	Dry weight (g)	Grain volume (cm^3)	Pore volume (cm^3)	Porosity (%)	Permeability (mD)
S1	4.05	3.833	94.965	35.852	10.918	23.344	581.76
S2	4.05	3.830	94.64	35.714	10.964	23.489	534.56
S3	4.051	3.833	95.057	35.908	10.88	23.254	470.21
S4	4.075	3.832	95.851	36.479	10.513	22.372	469.41
S5	3.993	3.833	93.234	35.684	10.395	22.56	450.25

Table 2b
ICP-OES analyses for digested core samples.

	mg. L^{-1}				
	Si	**Na**	**K**	**Ca**	**Mg**
rock digest (top)	0.02	0.556	4.20	0.168	0.236
rock digest (middle)	0.017	0.577	4.14	0.157	0.219
rock digest (bottom)	0.025	0.571	4.13	0.184	0.270

experiment was conducted to determine the mechanism responsible for EOR. The spontaneous imbibition tests were conducted using high-temperature Amott cells provided by Sagopec Energies International Inc, University of Calgary, Canada, with a volume capacity of approximately 400 ml. They were equipped with a graduated glass tube to directly measure the recovered oil from the cores. The recovery factor was determined based on the maximum volume of recovered oil per unit time. All spontaneous imbibition tests in this study were performed with no initial water saturation [50].

This experiment consisted of several stages, as detailed in the supporting information (SI3). After saturation of cores in oil, the cores were aged in an oven to alter the wettability of the cores to oil-wet. The aged cores were then washed with n-heptane to remove excess oil from the surface. Subsequently, the cores were placed in imbibition cells and filled with either brine or a low concentration of each nanofluid (approximately 0.005 wt%). The Amott cells, which contained the saturated cores and various fluids, were placed in an oven set at a temperature of approximately 60 °C [25].The imbibition test for the cores was continued until no further oil could be recovered. The volume of oil discharged from the cores was recorded to calculate the oil recovery as a percentage of the original oil in place, as shown in equation below [51].

$$OR = \frac{V_o \rho_o}{M} \times 100\%$$

Where *OR* represents the percentage of oil recovery from the cores after the imbibition test, V_o denotes the volume of oil discharged from the cores, ρ_o represents the density of the crude oil, and M is the difference in mass of the cores before and after saturation with crude oil.

3. Result and discussion

The surface of commercial SiO_2 NPs was functionalised by hydrophilic polymer coating (PEI) and hydrophobic moieties (TOS). The modification approaches employed here used cost-effective, commercially-sourced SiO_2 powders and simple, one-step procedure without the use of any binder or surfactant additives or necessity for pre-functionalisation with chemical handles, which is different from what has been reported elsewhere [52–54]. For modification with PEI, the PEI polymer was coated onto the surface of hydroxy-terminated SiO_2 NPs in aqueous solution. Interaction between the SiO_2 surface and the PEI coating are likely dominated by non-covalent, reversible interactions, such as hydrogen bonding and electrostatic interactions between depronated hydroxy-groups on the SiO_2 surface and protonated amine groups on the PEI polymer chain backbone. For modification with TOS, the modification agent was reacted with hydroxy-terminated SiO_2 NPs in non-aqueous cyclohexan solution. Interactions between SiO_2 surface and TOS are likely dominated by irreversible, covalent binding, based on condnesation reactions between the ethoxy groups of the TOS compound and the hydroxy groups on the SiO_2 surface. The schematic representation for the interaction mechanism between PEI and TOS and SiO_2 NPs can be seen in Fig. 1.

3.1. SiO_2 NPs modification with PEI and TOS agents

3.1.1. SEM/TEM analysis

The morphology of the prepared particles was obtained, using TEM) and SEM. Figs. 2 and S3 shows the TEM images of the unmodified SiO_2 NPs as well as modified PEI-NPs, and TOS-NPs, while Figure S4 shows the corresponding SEM images. TEM imaging shows no noticeable difference in the shape and size of the SiO_2NPs before and after the functionalisation with PEI and TOS, with all NPs types exhibiting roughly spherical morphology with an average diameter of the primary NPs of approximately 20 nm. For the unmodified nanopartciles, EDX spectra (Figure S5) confirmed the presence of silicon and oxygen for SiO_2 NPs, while for PEI-NPs it showed the presence of additional nitrogen, in line with presence of PEI on the nanopartcile surface. For TOS-NPs a slightly larger relative quantity of Si comnpared to the unmodified SiO_2-NPs, provides an indication of successful TOS-functionalisation. More generally, the obtained results (TEM, SEM, and EDX) confirmed that the morphology, structure, and shape of the particles are not impacted after nanoparticle modification.

3.1.2. Brunauer-Emmet-Teller (BET) results

The textural properties and the specifications of the SiO_2 NPs, PEI-NPs, and TOS-NPs were assessed by BET techniques. Figure S6 shows the adsorption and desorption isotherms for the SiO_2 NPs before and after functionalisation. All the isotherms are similar to those of type II [55]. When adsorption occurs on nonporous powders or powders with pore diameters larger than micropores (meso- or macroporous), type II isotherms are most commonly encountered. Therefore, functionalizing Si NPs with PEI and TOS agents resulted in a significant decrease in surface area as illustrated in the Table 3. This decrease can be attributed to the presence of these agents on the surface of SiO_2NPs, which could potentially affect the adsorption and diffusion of the N_2 molecules into the internal pores.

3.1.3. FTIR analysis

FTIR measurements were carried out for the prepared NPs before and after grafting to confirm the PEI/TOS functionalisation on the surface of the SiO_2 NPs (Fig. 3a).

For all samples, IR peaks were obtained at arround 1100 cm^{-1} and 800 cm^{-1} which were attributed to the Si-O-Si asymmetric stretching vibration [56]. The peaks around 470 cm^{-1} are attributed to the Si-O bonds [57]. For the PEI-NPs, additional absorption bands were observed at around 3000 cm^{-1} and 3438 cm^{-1} which can be assigned to the C–H and N–H stretching vibrations, confirming the presence of a PEI coating [58]. The presence of a PEI coating is further confirmed by the observation of C-N stretching and N–H bending modes at 16200 cm^{-1} and 1360 cm^{-1} for PEI-Si NPs [59]. The presence of these identified peaks confirms the presence of the amine containing PEI on the surface of the SiO_2 NPs.

For the TOS-NPs, absorption bands at atround 1400 and 2900 cm^{-1}

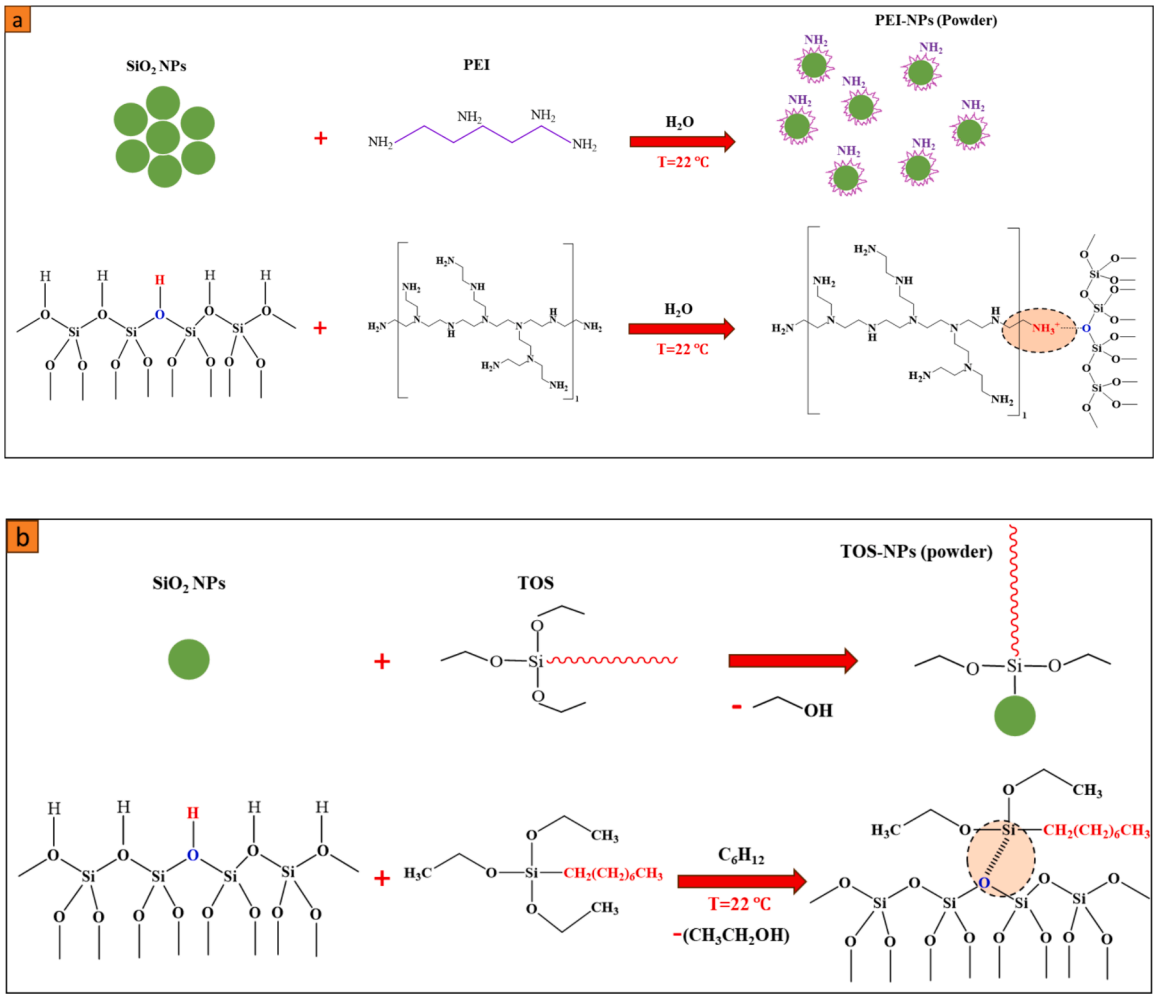

Fig. 1. Simple schematic representation for modification of commercial SiO_2 **NPs** with (a) PEI, and (b) TOS, respectively.

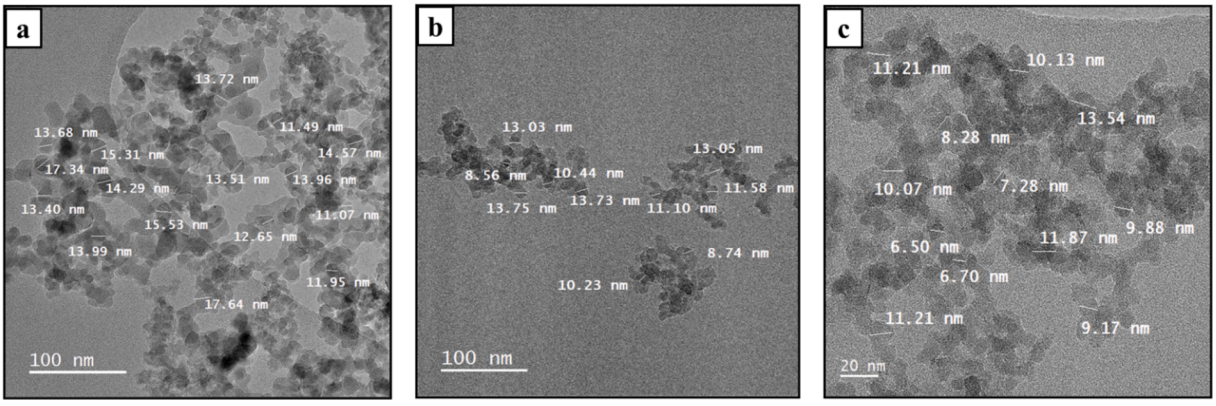

Fig. 2. TEM images for (a) SiO_2 NPs, (b) PEI-NPs, and (c) TOS-NPs. (For interpretation of the references to colour in this figure legend, the reader is referred to the web version of this article.).

Table 3
The BET surface area and the estimated particle sizes obtained by BET, TEM, and DLS analyses for SiO_2 NPs, PEI-NPs and TOS-NPs.

Sample	BET surface area (m^2g^{-1})	particle size obtained by TEM (nm)
SiO_2 NPs	238	10–20
PEI-NPs	92.13	10–20
TOS-NPs	77.5	10–20

were attributed to C–H bending and C–H stretching vibrations, respectively, indicating the presence of alkyl group from the TOS agent [58,60,61]. Hence, the aforementioned bands observed in the PEI-NPs and TOS-NPs spectra confirm the successful functionalisation of the SiO_2 NPs with these two agents in all the different prepared samples (Figure S7).

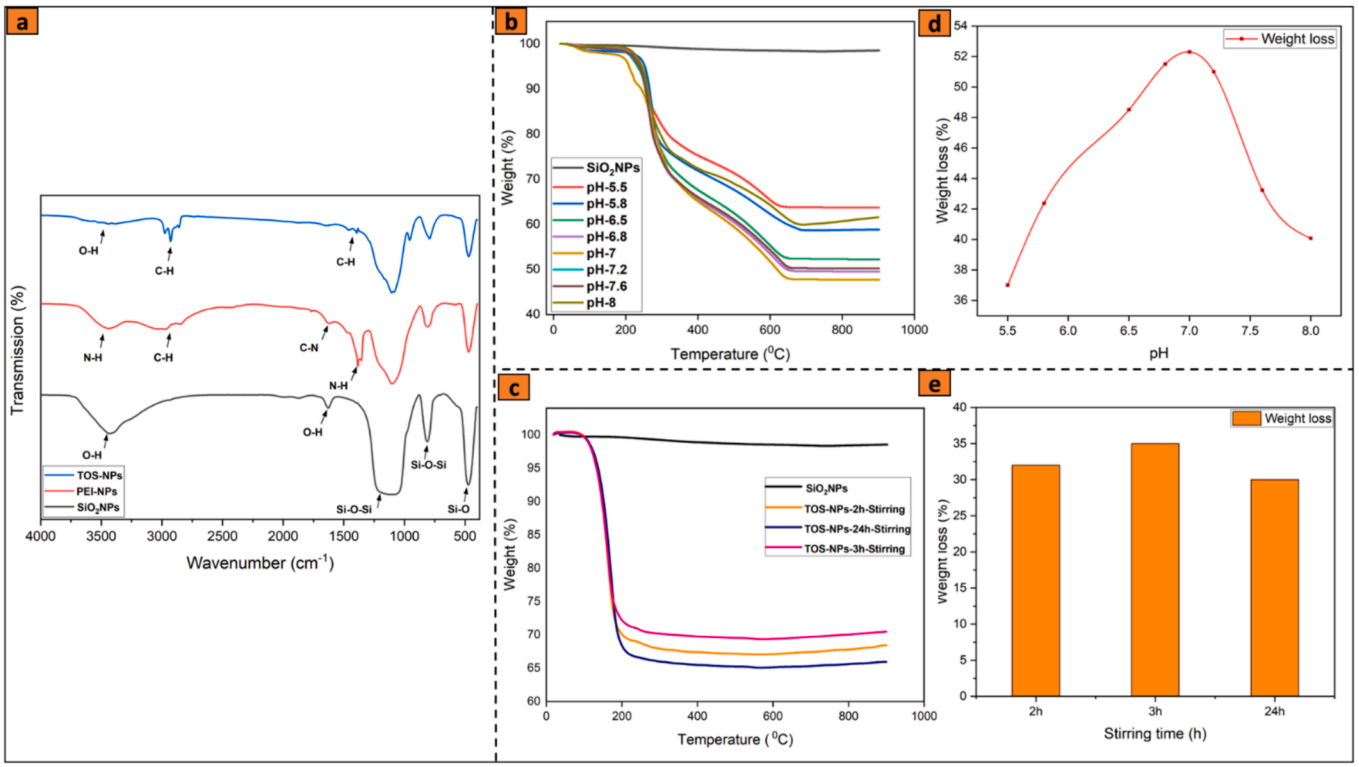

Fig. 3. (a) FTIR spectroscopy for SiO_2 NPs, PEI-NPs, and TOS-NPs at framework regions of 400–4000 cm^{-1}, TGA thermograms for SiO_2 functionalised-PEI-NPs (b) and -TOS-NPs (c), (d) the effect of pH on the weight loss for PEI-NPs, and (e) the effect of stirring time on the weight loss of TOS-NPs.

3.1.4. TGA analyses

TGA measurements were carried out for the SiO_2 NPs before and after grafting to quantify PEI and TOS content after modification. Fig. 3b and 4c show the TGA thermograms before and after the functionalisation of the SiO_2 NPs. As part of optimising the modification procedures for the PEI-NPs and TOS-NPs, a range of samples were prepared and analysed by TGA. Specifically, for PEI-modification, the impact of pH was studied (Fig. 3b and 3d; PEI-NP samples prepared at pH 5.5–8), as pH is likely impacting the electrostatic interactions between PEI and SiO_2 surface. For TOS modification, the impact of stirring duration was investigated (Fig. 3c and 3e; TOS-NP samples prepared at stirring for 2–24 h), in order to test when the reaction of TOS with the NPs is completed.

For all samples, two distinct weight loss domains are observed. The first one is from 25 to 150° C, obtained due to surface dehydroxylation or moisture content loss. The second domain was from 150 to 900 °C, which was obtained due to the thermal decomposition of the organic substance that existed or loaded in the SiO_2 NPs surface. The amount of loaded PEI agent on the surface of the virgin SiO_2 NPs in the second temperature domain showed an increase in the total mass loss by improving the polymer loading during the synthesis, which occurred by varying the pH from 3.5 to 8 (Fig. 3d). The improvement in weight loss is evident, rising from 37 % at pH 5.5 to 52 % at pH 7. Subsequently, it gradually declined, reaching 40 % at pH 8, as illustrated in Fig. 3d.

On the other hand, stirring time did not notably affect the loading of the TOS agent onto the surface of the SiO_2 NPs on the timescales probed. The total mass loss varied from 30 % to 35 % when the stirring time increased from 1 h to 3 h, as depicted in Fig. 3e. TGA-analyses indicated that PEI-NPs has high thermal stability up to 200 °C. In contrast TOS-NPs began to decompose at approximately 150 °C, however it remains suitable for the use within the usual temperature range of EOR reservoirs (typically less than 120 °C). Based on these findings, all PEI-NP samples discussed in the remainder of this work were prepared at pH 7, and all TOS-NP samples were prepared at a stirring time of 3 h.

3.2. Optimising dispersion stability of modifies SiO_2

3.2.1. Zeta potential measurements for different nanofluids

NPs tend to aggregate or flocculate due to the attractive forces between the particles. The aggregation of NPs can lead to a decrease in their stability and can affect their applications for EOR [62]. Thus, the functionalisation of the NPs with different agents can prevent their aggregation [63]. ZP plays a crucial role in determining the stability of NPs. NPs with a considerable positive (ZP >+30 mV) or negative (ZP<-30 mV) charge have a strong electrostatic repulsion, leading to better stability and reducing the chance of aggregation and precipitation, while particles with a low ZP (between −30 and + 30 mv) tend to aggregate and flocculate due to the increase of the attractive forces between them, resulting in instability [64].

Around 0.005 g of each set of prepared NPs was dispersed in 100 ml of DW for the ZP measurements. Fig. 4a shows the ZP measurements for PEI-NPs samples that prepared under different pH conditions. The highest recorded value, +73.9 mV, was observed for the sample prepared at pH 7. This positive surface potential is attributed to the fact that majority of the amine groups of the PEI are likely to be protonated at this pH [65]. This increase in ZP is also consistent with the presence of a large amount of PEI on the NPs surface. For the TOS-NPs samples, adjusting the pH to 9 has slightly improved the ZP values. As shown in Fig. 4b, the highest ZP value was obtained for the 3 h-stirring sample with −47.2 mV. This significant increase in ZP after functionalisation with TOS aligns with findings reported in the literature [40,41]. The likely mechanism behind this increase involves the hydrolysis of the TOS-based ethoxy groups in aqueous solution. This hydrolysis leads to the formation of additional hydroxyl groups, with two hydroxyl groups per functionalisation site (see the suggested structure in Fig. 5b). These groups, can deprotonate, contributing to an increase in the negative surface charge. Determining the mechanism for highly negative ZP of the TOS-NPs is beyond the scope of current study and can be the subject of future investigation. The results indicate that functionalization with

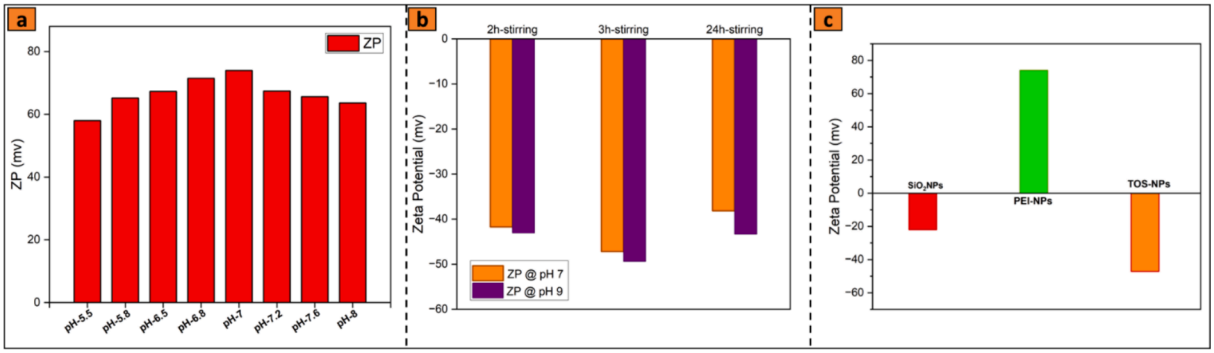

Fig. 4. ZP distributions, (a) for the different prepared PEI-NPs samples at different pH, (b) for the different prepared TOS-NPs at different stirring time and at neutral pH and pH 9, (C) for the unmodified SiO_2 NPs and the selected PEI-NPs and TOS-NPs.

PEI and TOS enhanced the stability of the SiO_2 NPs, by shifting the surface charge from –22 mV to + 73.9 mV and –47.2 mV, respectively (see Fig. 4c).

3.2.2. *The hydrodynamic size distribution for different nanofluids*

The NPs in suspensions tend to aggregate or agglomerate, affecting their stability and performance as EOR agents. Dynamic Light Scattering (DLS) is a technique used to measure the hydrodynamic size distribution of the suspended particles in solution. The virgin SiO_2 NPs as reported by many researchers tend to aggregate in aqueous conditions [29,31,66,67]. However, functionalising the SiO_2 NPs with different stabilizing agents can improve their stability and reduce their tendency to aggregate. DLS tests were conducted on both non-grafted and grafted SiO_2 NPs to determine the average hydrodynamic size distribution. Approximately 0.005 g of each set of prepared NPs was dispersed in 100 ml of DW. Figure 5a presents the hydrodynamic size distribution of SiO_2 NPs, PEI-NPs (pH=7), and TOS-NPs (3 h-stirring). The average size for the unmodified SiO_2 NPs was approximately 250 nm, suggesting aggregation (see also supporting information, Figure S9-a). In contrast, PEI-NPs, and TOS-NPs considerably improved stability in aqueous dispersion, with the average size of around 50 nm and 90 nm, respectively. These findings corroborate the outcomes obtained from the ζ-potential analyses. The larger aggregate size of TOS-NPs in aqueous dispersion, compared to the PEI-NPs, is attributed to the partially hydrophobic character of the grafted TOS functionalities (in contrast to the fully hydrophilic polymer coating of the PEI-NPs). It is however worth noting that TOS functionalisation nevertheless leads to a substantial reduction of aggregate size compared to the unmodified SiO_2 NPs. This observation suggests some hydrophilicity of the TOS-NPs (in line with the ZP results for TOS-NPs), based on the hydrolysis of the TOS-based ethoxy groups and subsequent formation of Si-OH functionalities (see Fig. 5b).

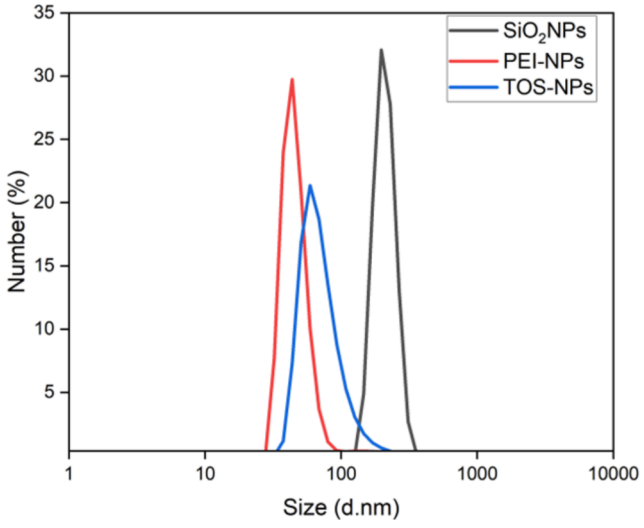

Fig. 5a. The size distribution of the SiO_2 NPs, PEI-NPs, and TOS-NPs, with pH values of the resulting particles dispersion being 5.5, 6, and 4.5, respectively.

3.2.3. *Selection of Low-Salinity water (LSW)*

The ZP is a crucial indicator of the stability of colloidal systems [68]. By measuring ZP in sand particles with different brine solutions, we can identify a brine formulation that is most suitable for the EOR techniques. Selecting a brine with a favourable ZP improves NPs dispersion and transport within the reservoir, ultimately maximizing oil recovery efficiency [45,69]. Fig. 6 depicts the ZP measurements for various brine solutions, each containing 0.5 g of sand. The highest ZP value was achieved with BS-B, comprising NaCl at 500 ppm, measured at −52 mV. Where the lowest ZP value was obtained for brine containing divalent ions. Consequently, BS-B was designated as LSW, and it will serve as the dispersant solvent for the NPs in all forthcoming experiments.

It worth noting that the aforementioned approach aligns with findings from the reported studies literatures [40,45] that highlight the significant impact of water salinity on NPs stability, which is essential for effective EOR application. In this essence, the higher salinity brines, especially those containing divalent cations, showed a significant effect on ZP compared to the lower salinity solutions that provided more favourable ZP for NPs dispersion and stability [40,45].

3.2.4. *The effect of nanoparticle concentration on the stability in LSW*

Nanoparticle (NP) concentration plays a crucial role in disjoining mechanisms, directly impacting oil recovery. For example, increasing NP concentration can enhance disjoining pressure and Brownian motion, leading to improved oil detachment through wettability alteration of the rock surface [70]. However, it is important to note that a high particle concentration does not always result in higher oil recovery. This inconsistency can be attributed to potential issues such as nanoparticle aggregation and pore clogging at high nanoparticles concentrations [28,71]. Fig. 7a, 7b, and 7c. illustrates the effect of different concentrations of virgin and functionalized silica NPs (25/50/100/500 ppm) dispersed with LSW on their stability, evaluated using ZP measurement. Among all the NPs, the 50-ppm concentration demonstrated the most favourable results for ZP, with values around + 45 mV for PEI-NPs and −40 mV for TOS-NPs, prompting its selection for studying the effect of high temperature and pH, as well as for the EOR experiment.

3.2.5. *The effect of pH on the stability of the nanofluids in LSW.*

Table 4 illustrates the impact of pH on the stability of the prepared NPs in LSW. The analyses revealed different behaviours across the different prepared NPs. Pure SiO_2 NPs are characterized by large hydrodynamic sizes and relatively low ZP values across all pH levels, indicating general tendency to form large aggregates independent of pH.

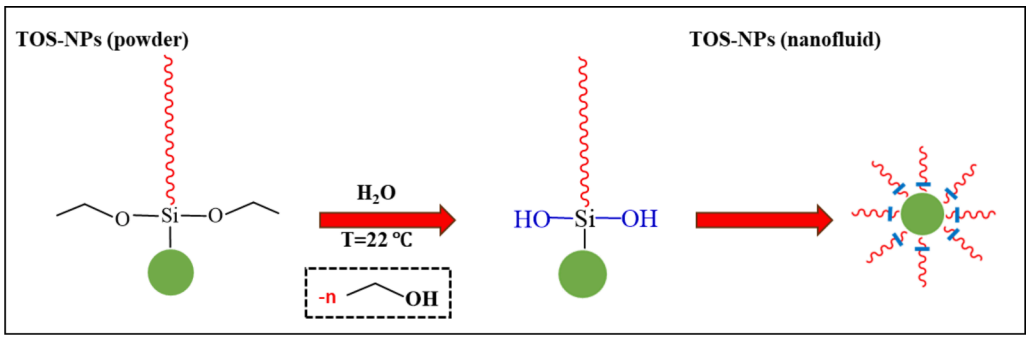

Fig. 5b. Hydrolysis of TOS-based ethoxy groups, resulting in an increase in Si-OH groups (blue, likely introducing some hydrophilic character) next to the TOS-based octyl groups (red, providing hydrophobic/oleophilic character).

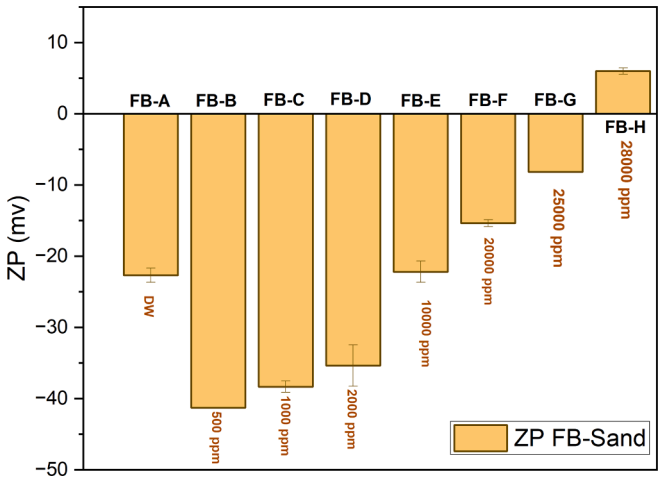

Fig. 6. ZP distribution for the different brine solutions with 0.5 g of sand.

In contrast, PEI-NPs exhibit the smallest hydrodynamic particles sizes and relatively high positive ZPs. Smaller particle sizes were observed at low to medium pH due to protonation of amine groups and resulting electrostatic particle stabilisation. TOS-NPs display slightly larger hydrodynamic sizes compared to PEI-NPs, but smaller particles sizes than pure SiO_2 at all pH levels. Smaller sizes were observed at medium to high pH due to deprotonation of Si-OH groups of the TOS functional groups. Figure S11 presents the size distribution for LSW with SiO_2 NPs, PEI-NPs, and TOS-NPs at different pH.

3.2.6. *The effect of temperature on the stability of the nanofluids in LSW*

The reservoir temperature typically ranges from 20 to 120 °C [72–75], significantly higher than surface conditions. This necessitates that NPs used in such environments maintain their effectiveness at these elevated temperatures. It is well reported that NPs tend to agglomerate as temperature increases, primarily due to a decrease in ZP, which adversely affects their stability and dispersion within fluid medium [70]. To check the suitability of NPs for injection in oil reservoirs, their stability measurement was conducted at a reservoir temperature of 60 °C [25], using selected concentrations of NPs and selected LSW. Fig. 8 presents both the ZP and size distribution of the nanoparticles, tested at both room and elevated temperatures. At 60 °C, PEI-NPs maintained a high positive ZP of + 30 mV, indicating good stability, whereas the ZP of TOS-NPs was −21 mV, suggesting moderate stability. In contrast, the virgin SiO_2 NPs displayed a significant decline in stability evidenced by ZP of around −3 mV, which is indicative of poor dispersion at the reservoir temperature. Furthermore, PEI-NPs and TOS-NPs exhibited minimal changes in size, indicating strong resistance to thermally induced aggregation. In contrast, the size of unmodified SiO_2 NPs increased notably, by about 150 nm, showing a pronounced susceptibility to thermal effects. This differential behaviour highlights the importance of selecting NPs with favourable thermal stability for successful EOR application in reservoirs temperature.

Table 4
ZP and the average aggregate size for SiO_2 NPs, PEI-NPs, and TOS-NPs in LSW at different pH.

	pH 3		Baseline pH		pH 9	
Samples	**ZP (mV)**	**DLS (nm)**	**ZP (mV)**	**DLS (nm)**	**ZP (mV)**	**DLS (nm)**
SiO_2 NPs	−3.7	540	−16.6 (pH5.5)	302 (pH5.5)	−2.9	525
PEI-NPs	+26.7	62	+46.5 (pH6)	56 (pH6)	+37.2	124
TOS-NPs	−5.9	452	−42.4 (pH4.5)	62 (pH4.5)	−35.9	133

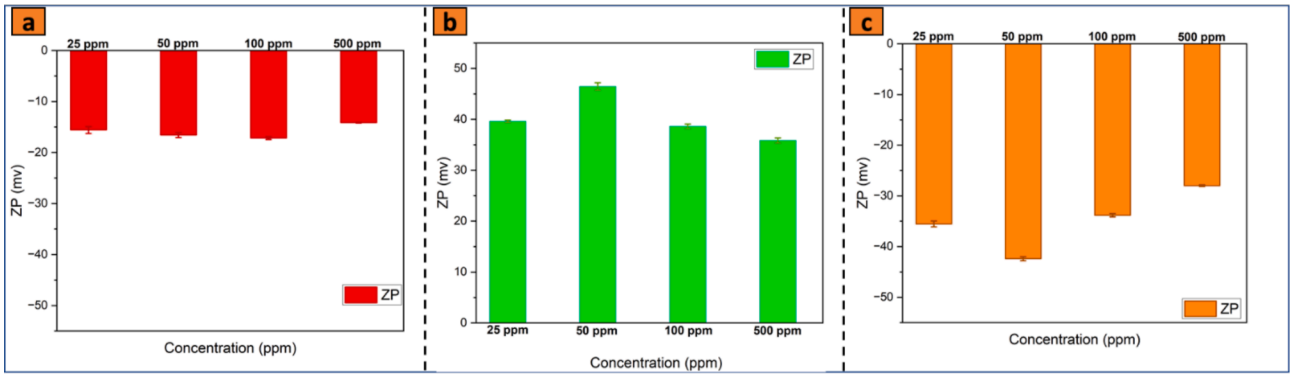

Fig. 7. The effect of the concentration on the zeta-potential and hydrodynamic aggregate size of (a) the virgin SiO_2 NPs, (b) PEI-NPs, (c) TOS-NPs in LSW.

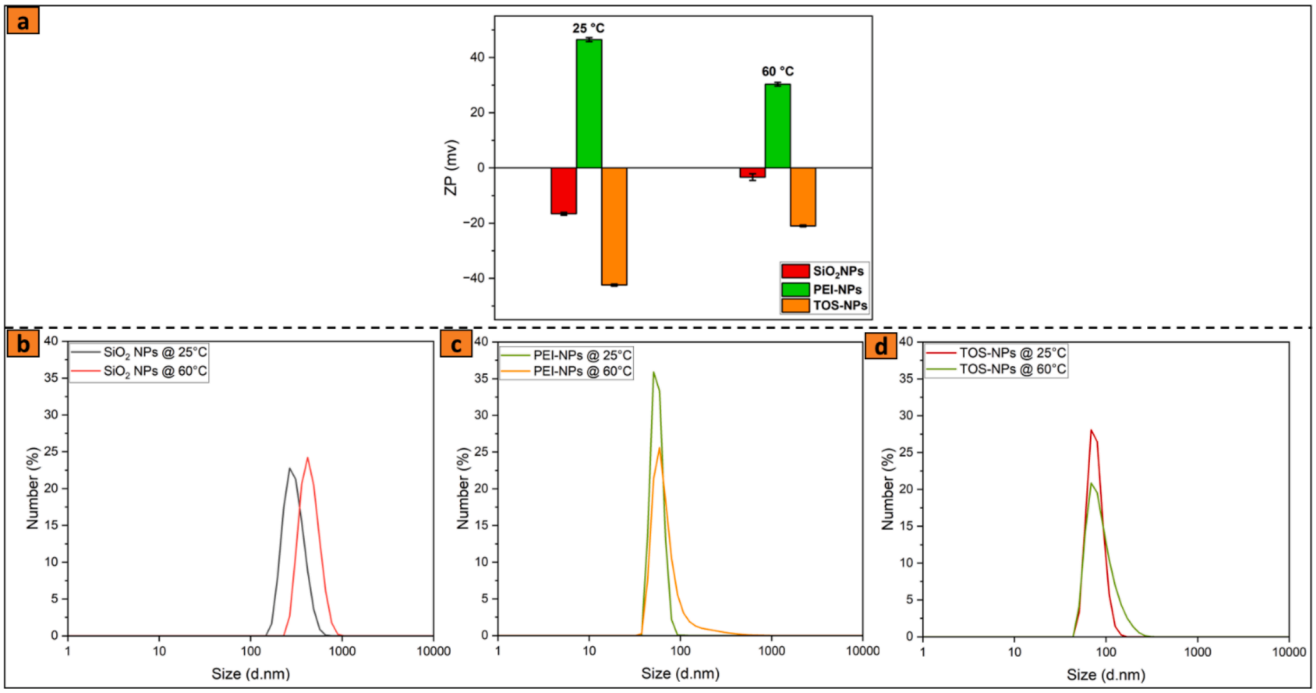

Fig. 8. Zeta potential and Size distribution of NPs at room and high temperature; (a) ZP distribution for all samples, (b) size distribution for SiO_2 NPs, (c) PEI-NPs, and (d) TOS-NPs.

3.3. Enhanced oil recovery measurements

3.3.1. Contact angle analysis

The contact angle measurement is an important quantitative technique for assessing surface wettability and determining its behaviour in the presence of different phases. Reservoirs are naturally water-wet, but they transition to oil-wet happens due to the deposition of heavier hydrocarbons on the rock surface. Regarding the three-phase contact angle, wettability is typically classified into three categories: water-wet if the contact angle is between 0 and 75°, intermediate-wet between 75 and 105°, and oil-wet between 105 and 180°, when measured towards the denser phase [76]. Our study aims to investigate whether the nanofluids can alter the rock surface wettability from oil or intermediate-wet to water-wet. Therefore, in this study, the contact angle is measured towards the less dense phase, with higher contact angles (>90°) defining water wetness, while lower contact angles (<90°) indicate oil-wetness. Contact angle measurements were carried out on polished sandstone substrate before and after aging the cores in crude oil following the protocol mentioned before (section 2.5.1). The sandstone samples were naturally strongly water-wet, and we attempted to change their wettability to simulate reservoir conditions (oil-wet) by aging them in crude oil.

Fig. 9a and 9b show that the contact angle before and after aging. It can be clearly seen that the contact angle reduced from 158° to 27° after aging, indicating the wettability alteration of the standard substrate from water-wet to strongly oil-wet due to the aging process. This change can be explained by the partial adsorption of polar components in the crude oil on the surface of the sandstone. Fig. 9c-e show the oil droplet contact angle measurement of the three-phase oil-aqueous-rock interface at room temperature with different nanofluids. The estimated contact angles were around 94°, 16°, and 165°, for SiO_2NPs, PEI-NPs, and TOS-NPs, respectively (Fig. 9f). The presence of TOS-NPs significantly changed the wettability of the rock surface to strongly water-wet. Meanwhile, virgin SiO_2 NPs changed the wettability to intermediate wet, whereas the surface remained strongly hydrophobic and extremely oil-wet in the presence of the PEI-NPs. Depending on the type and surface charge of the NPs (before and after functionalisation), their affinity to the rock surface can be altered, forming a larger or smaller wedge film based on their electrostatic repulsive/attraction forces. The largest wedge film leads to detaching more oil droplets, then making the surface more water wet.

On the other hand, the measurement of the IFT between the crude oil droplet and the different nanofluids is important for the imbibition test in terms of understanding the responsible mechanism for oil recovery using NPs. A high IFT indicates low oil mobility, whereas a low IFT indicates high oil mobility, leading to improved oil recovery. Fig. 10 shows the IFT between the crude oil droplets and the different prepared imbibition fluids over time. The equilibrium IFT values for oil-DW, oil-LSW, and oil- BS-G were 24.09 ± 0.04, 19.61 ± 0.04, and 2.05 ± 0.02 mN/m, respectively. Consequently, the IFT between oil and BS-G reduced by 75 % compared to that of oil and LSW, which reduced by just 18.6 %. The observed reduction can potentially be attributed to the higher concentration of salt ions at the interface with BS-G. For oil in LSW mixtures, the IFT measurement in the presence of virgin SiO_2 NPs was around 19.9 ± 0.04 mN/m, i.e., almost identical to the IFT in absence of SiO_2 NPs. These results confirm previous observations by other researchers regarding the low IFT reduction achieved using virgin SiO_2 NPs [77]. However, the IFT with PEI functionalized SiO_2 decreased from 19.6 mN/m to 5.2 mN/m (a decrease of about 78 %). This significant decline can be attributed to the adsorption of PEI-NPs at the interface between the oil droplet and water. The IFT using the TOS-NPs nanofluid was measured at 18.6 mN/m, indicating a reduction of approximately 5.1 %.

3.3.2. Oil recovery by spontaneous imbibition test

The efficiency of the different prepared fluids with and without NPs for enhancing oil recovery was evaluated using the spontaneous imbibition tests. The test was carried out under atmospheric pressure and at reservoir temperature (60° C). Various aged and saturated Berea sandstone cores with crude oil were placed inside the Amott cells filled with different prepared imbibition fluids. Table S4 shows the oil recovered from the different aged cores using various prepared imbibition fluids. The imbibition test was conducted for 25 days, with most of the saturated oil being recovered in the first two days, followed by lower oil

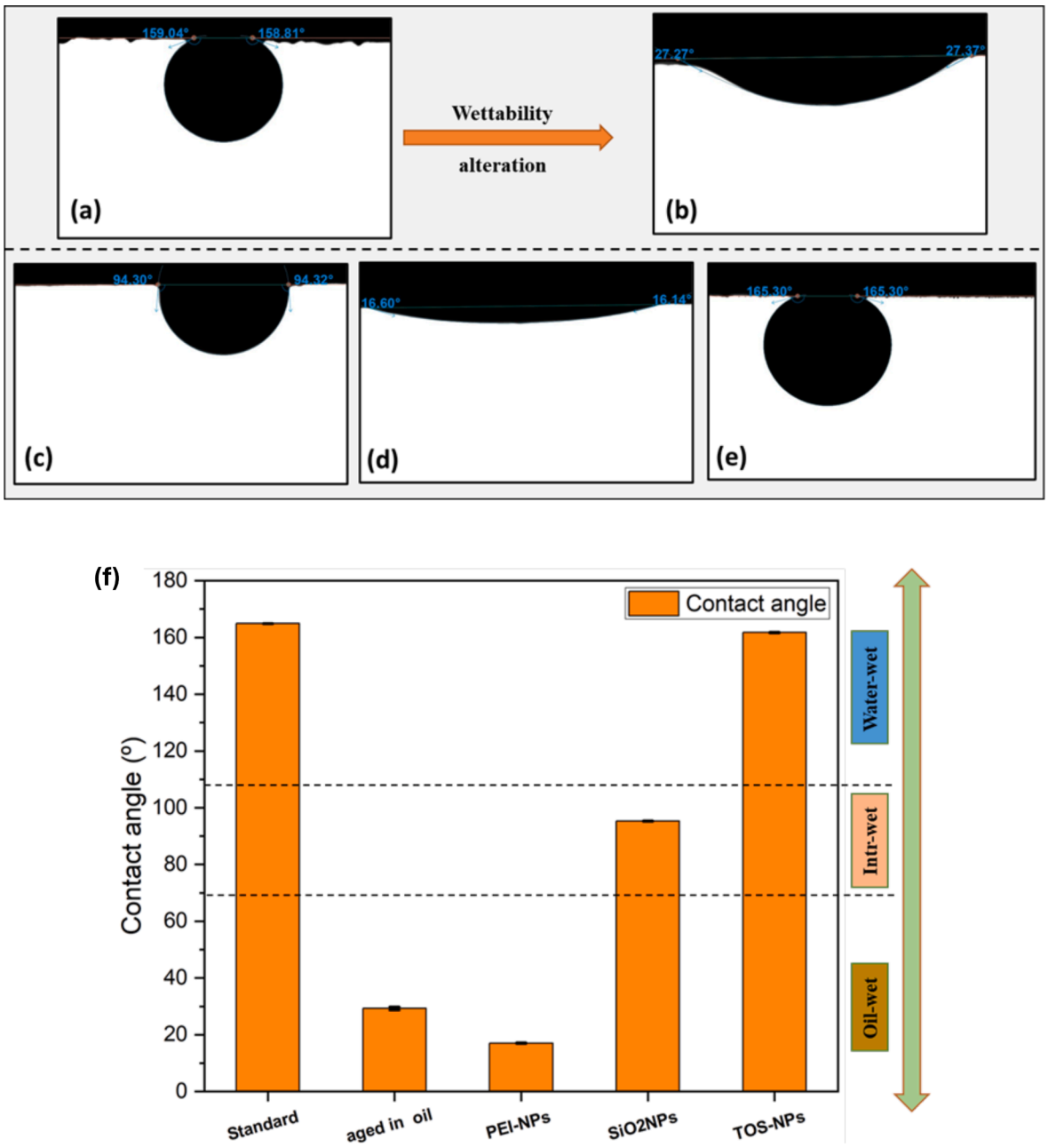

Fig. 9. Contact angle measurement (a) before and (b) after aging in crude oil, (c) in the presence of SiO_2 NPs, (d) PEI- NPs, (e) TOS-NPs and (f) the summary results.

recovery for all the imbibition fluids until day 18. Fig. 11 illustrates the performance of functionalized and non-functionalized SiO_2 NPs for oil recovery from the aged and saturated Berea sandstone cores through the spontaneous imbibition test, compared to BS-G and LSW. When LSW was used as the imbibition fluid, 54.93 % of the original oil from the saturated core was recovered, reaching a plateau on day 6. The oil recovered by BS-G as the imbibition fluid was approximately 56.17 % and reached a plateau on day 10. Moreover, 53.44 % of the original oil was recovered from the saturated core by the nanofluid containing SiO_2 NPs, reaching a plateau after a week of the imbibition test. However, the imbibition fluid with PEI-NPs exhibited very low oil recovery at about 9.82 % and reached a plateau on day 6. Conversely, the imbibition fluid with TOS-NPs showed the highest oil recovery compared to all the previous imbibition fluids, with a percentage of 64.92 %, reaching a plateau after approximately 16 days. The results of the spontaneous imbibition test correlates with the contact angle measurements, indicating that functionalized $SiO_2$with TOS agent has changed the wettability of the rock surface from oil-wet to strongly water-wet, thereby improving oil recovery. Figure S15 presents the Amott cells used for the imbibition test: (a) on the first day and (b) after 24 days. Figure S16 displays several oil droplets on the surface of the imbibed cores using TOS-NPs, confirming wettability alteration of the rock surface following the application of TOS-NPs. The effective performance of TOS-NPs may be attributed to the presence of a combination of hydrophobic (octyl) and hydrophilic groups (Si-OH) in the TOS functionalities. In the cell containing PEI-NPs nanofluid, a layer of sand was observed to have been released from the core sample, as depicted in Fig. 12. This poor performance seems unexpected; it might indicate that PEI is not well attached to SiO_2 (only electrostatic interactions). Consequently, PEI can detach and facilitate dislodging/solubilising small sand grains, which can lead to pore clogging during the oil release and thus cause mechanical entrapment inside some pores and on the surface of the rock, significantly lowering oil recover. For more clarification of results, we have carried out an additional experiment where the PEI-NP were suspended in aqueous solution

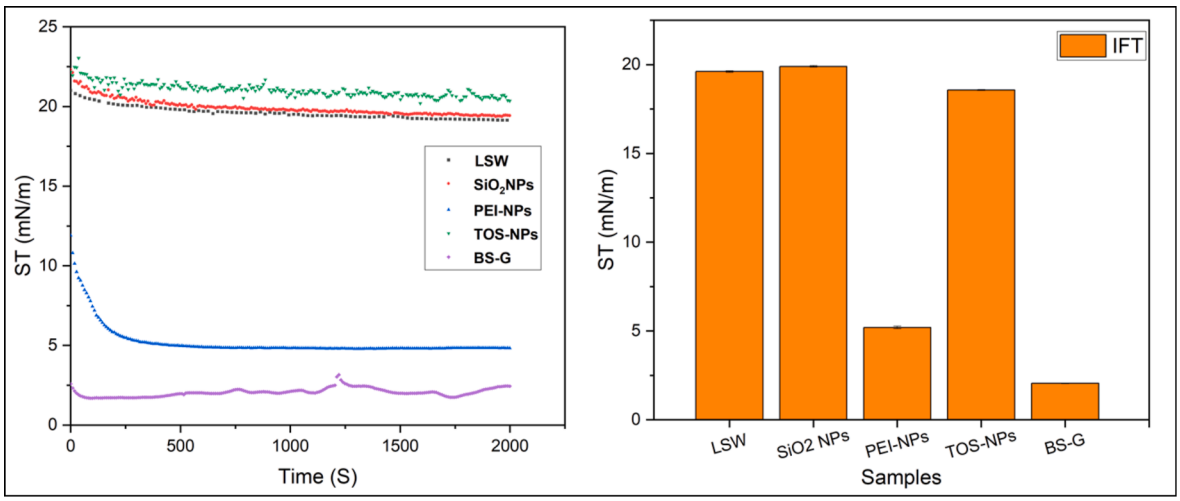

Fig. 10. IFT measurement between crude oil droplet and different imbibition fluids.

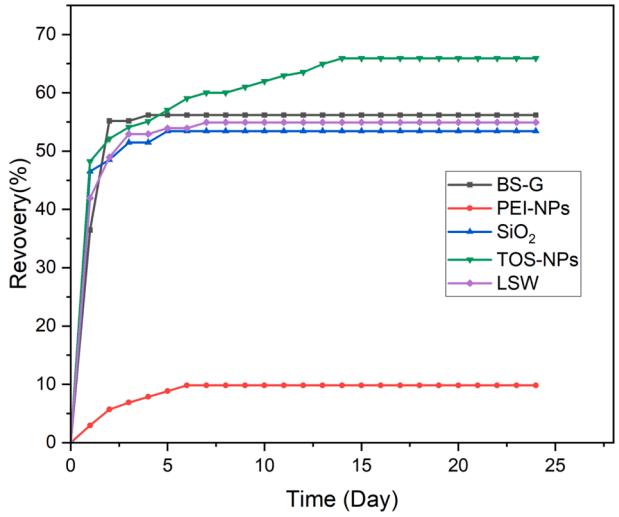

Fig. 11. Percentage of Oil Recovered from Saturated Berea Sandstone Cores Over Time by Spontaneous Imbibition Test with Different Imbibition Fluids.

under identical conditions as those used in the imbibition test (see Figure S17a). The PEI-NP suspension was then left in dispersion for 7 days (the time when imbibition tests suggested that maximum EOR was reached, see Fig. 11). After this 'aging' process, the PEI-NP were isolated through centrifugation. TGA was then used to determine the amount of PEI remaining on the nanoparticle surface after aging for 7 days. The TGA results shown in Figure S17b, revealed that only 3 % PEI remained on the nanoparticle surface after 7 days in solution (compared to 52 % PEI in the as-synthesised PEI-NPs). This confirms that, at longer times in dispersion with cores, a substantial amount of PEI separates from the PEI-NPs. It is worth noting that aggregation of NPs was observed for the virgin SiO_2 NPs in different parts of the Amott cell, as illustrated in Fig. 12. This phenomenon could present challenges in larger-scale field applications.

After the imbibition test, the cores were dried and then crushed. Figure S18 illustrates the difference in colour between the reference core, which was not used for the imbibition test, and the other core sample after the imbibition test. The core imbibed by PEI-NPs nanofluid shows a browner colour, while the saturated cores treated by TOS-NPs show a lighter brown colour, correlating with the results obtained from the imbibition test. As a result, the latter finding proposes that the wettability change could be the dominant mechanism for EOR within the sandstone reservoir, stating that the synthesised TOS-NPs outperformed that of the PEI-NPs and unmodified SiO_2 NPs.

4. Conclusion

In this study, a family of environmentally friendly and cost-effective silicate nanomaterials, which are easy to prepare and functionalize, was utilized for the EOR studies. SiO_2 NPs were modified by surface functionalization with two different agents at room temperature and low pressure, without the use of any binding agents. Two novel agents were employed: branched amino-based polymer PEI and TOS agents marking the first application of these agents with SiO_2 NPs for EOR. The main finding of our study is that the TOS-NP nanofluid exhibited excellent oil recovery (65 %) during spontaneous imbibition tests (conducted under high temperature and saline conditions), indicating its potential for EOR applications. TOS-NPs nanofluids showed excellent stability and remarkable ability to change rock wettability. Although PEI-NPs exhibited substantial IFT reduction, they did not enhance oil recovery, suggesting that wettability alteration of the rock could be the primary mechanism responsible for improving oil recovery.

The study also led to several other interesting findings which include:

- Substantial TGA weight losses, characteristic IR peaks and reduction in BET surface area (~92 and ~ 77 m^2/g for PEI-NPs and TOS-NPs, respectively, compared to 238 m^2/g for unmodified SiO_2 NPs) confirmed successful functionalization of the SiO_2 NPs with PEI and TOS, respectively.
- Adjusting the pH of branched PEI polymers enhanced their loading onto the SiO_2 NPs' surface, with the most significant polymer loading occurring at pH 7, resulting in approximately 52 wt% PEI loading on the SiO_2 NPs. Modification of SiO_2 NPs with TOS was completed after 3 h reaction duration, resulting in approximately 35 wt% TOS loading.
- Electron microscopy imaging showed that PEI-NPs and TOS-NPs materials were composed from nearly spherical primary NPs with an average size of 10–20 nm.
- ZP measurements confirmed the enhanced stability of SiO_2 NPs after surface functionalization in aqueous solution. The stability was significantly improved, with ZP values shifting from −25 mV for virgin SiO_2 NPs to + 74 mV for PEI-NPs and to −47.2 mV for TOS-NPs. The ZP results are consistent with changes in aggregate size in aqueous solution, as measured by DLS, with the aggregates size reducing after nanoparticle modification from 250 nm (for virgin SiO_2) to 50 nm and 90 nm, for PEI-NPs and TOS-NPs, respectively. The stability of the prepared materials and reduction of aggregate

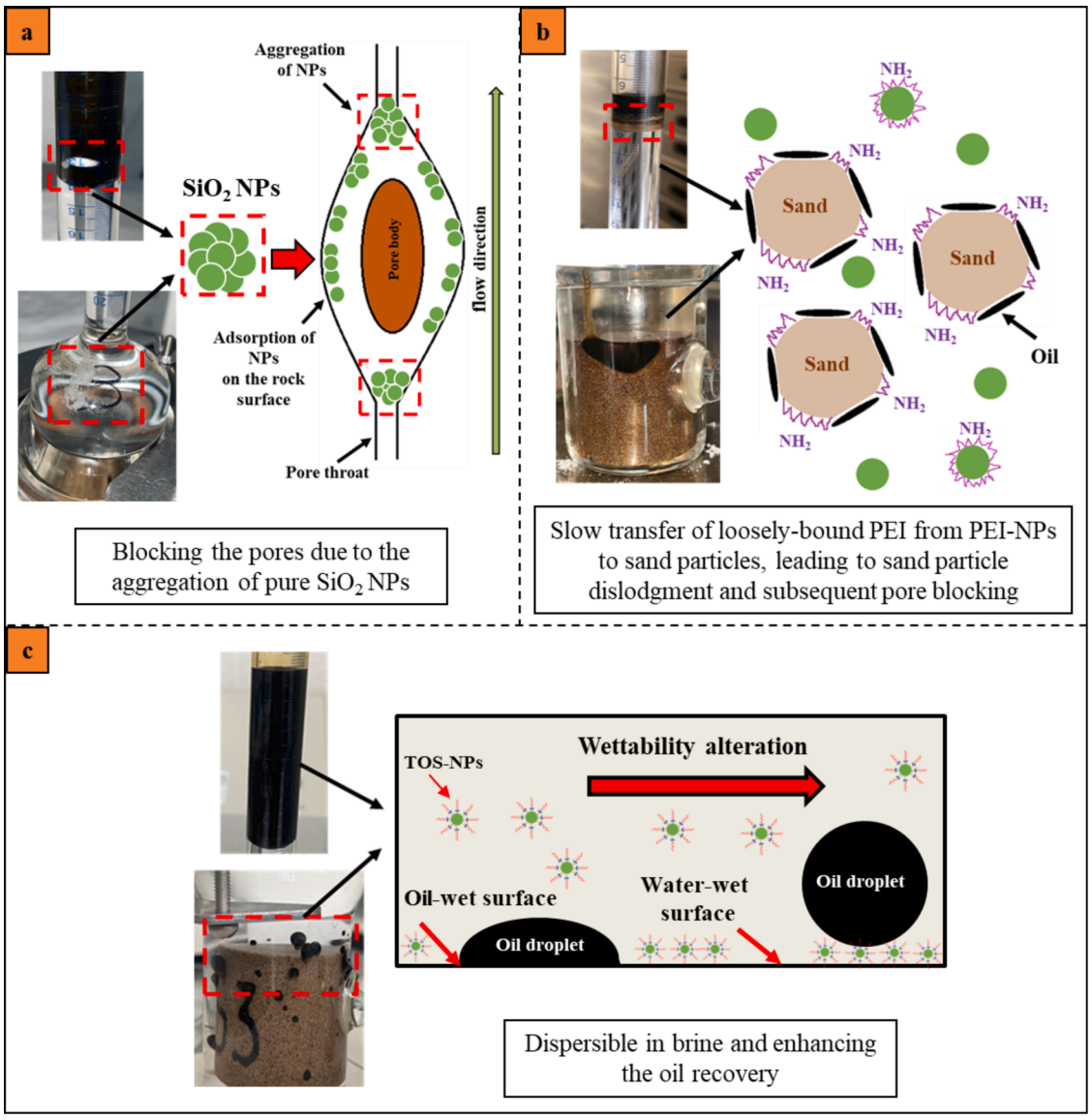

Fig. 12. Potential mechanism for EOR using different nanofluids, (a) SiO_2 NPs, (b) PEI-NPs, and (c) TOS-NPs.

size upon functionalisation was confirmed across various brine solutions and high temperatures (close to reservoir conditions).

- The nanofluid containing TOS-NPs altered the wettability of the sandstone substrate from strongly oil-wet (27°) to strongly water-wet (165°). Conversely, the contact angle between the nanofluid containing PEI-NPs and crude oil droplets was minimal, confirming their inability to alter the rock substrate's wettability.
- Surface modification of SiO_2 NPs with PEI significantly reduced the IFT by 78 % compared to a 5 % reduction achieved by modifying SiO_2 with TOS agent.
- The effective performance of TOS-NPs may be attributed to the presence of a combination of hydrophobic (octyl) and hydrophilic groups (Si-OH) in the TOS functionalities. In contrast, the PEI-NPs-based imbibition fluid showed the lowest oil recovery (9.8 %). Which might indicate that PEI is not well attached to SiO_2 (only electrostatic interactions). Consequently, PEI can detach and facilitate dislodging/solubilising small sand grains, which can lead to pore clogging during the oil release and thus cause mechanical entrapment inside some pores and on the surface of the rock, significantly lowering oil recovery, rendering these particles unsuitable for EOR.

CRediT authorship contribution statement

Louey Tliba: Writing – review & editing, Writing – original draft, Methodology, Investigation, Formal analysis, Data curation, Conceptualization. **Farad Sagala:** Writing – review & editing, Validation. **Afif Hethnawi:** Writing – review & editing, Conceptualization. **Paul W.J. Glover:** Writing – review & editing, Supervision, Methodology. **Robert Menzel:** Writing – review & editing, Supervision, Methodology, Investigation. **Ali Hassanpour:** Writing – review & editing, Supervision, Methodology, Investigation, Conceptualization.

Declaration of competing interest

The authors declare that they have no known competing financial interests or personal relationships that could have appeared to influence the work reported in this paper.

Data availability

Data will be made available on request.

Acknowledgement

The authors wish to express their deep appreciation to the following individuals for their substantial contributions: Dr. Ben Douglas, Mr. Mohamed Edokali, Dr. Karine Alves Thorne, Dr. Adrian Cunliffe from school of chemical and process engineering, Mr. Stuart Micklethwaite and Dr. Zabeada Aslam from Leeds Electron microscopy and spectroscopy centre (LEMAS). We are especially grateful to Mr. John Wyn Williams from the Leeds University School of Earth and Environment for his expert assistance with sample preparation.

Appendix A. Supplementary data

Supplementary data to this article can be found online at https://doi.org/10.1016/j.molliq.2024.125815.

References

[1] E.C. Donaldson, G.V. Chilingarian, T.F. Yen, Enhanced oil recovery, I: fundamentals and analyses, Elsevier, 1985.
[2] S. Kokal, A. Al-Kaabi, in: Enhanced Oil Recovery: Challenges & Opportunities, World Petroleum Council: Official Publication, 2010, pp. 64–69.
[3] H. Rashedi, et al., in: Microbial Enhanced Oil Recovery, 2012, pp. 71–88.
[4] N.A. Owen, O.R. Inderwildi, D.A. King, *The status of conventional world oil reserves—Hype or cause for concern?* Energy Policy 38 (8) (2010) 4743–4749.
[5] L. Romero-Zeron, Chemical Enhanced Oil Recovery (cEOR), A Practical Overview, InTech (2016).
[6] A.A. Olajire, Review of ASP EOR (alkaline surfactant polymer enhanced oil recovery) technology in the petroleum industry: Prospects and challenges, Energy 77 (2014) 963–982.
[7] R.M. Dean, et al., State-of-the-art laboratory methods for chemical EOR. SPE Improved Oil Recovery Conference, SPE, 2022. SPE-209351-MS.
[8] M.S. Kamal, et al., Review on polymer flooding: rheology, adsorption, stability, and field applications of various polymer systems, Polym. Rev. 55 (3) (2015) 491–530.
[9] E. Mahdavi, F.S. Zebarjad, Screening Criteria of Enhanced Oil Recovery Methods, in: A. Bahadori (Ed.), Fundamentals of Enhanced Oil and Gas Recovery from Conventional and Unconventional Reservoirs, 2018, pp. 41–59.
[10] Sun, X., et al., Application of nanoparticles in enhanced oil recovery: a critical review of recent progress, Energies,10 (3) (2017) 345.
[11] B.A. Suleimanov, et al., *Nanofluid for enhanced oil recovery*, Journal of Petroleum Science and Engineering 78 (2) (2011) 431–437.
[12] Zhang, T., et al. *Nanoparticle-stabilized emulsions for applications in enhanced oil recovery*. in *SPE improved oil recovery symposium*, 2010, OnePetro, SPE-129885-MS.
[13] L. Hendraningrat, S. Li, O. Torsæter, A coreflood investigation of nanofluid enhanced oil recovery, J. Pet. Sci. Eng. 111 (2013) 128–138.
[14] M.S. Alnarabiji, M.M. Husein, Application of bare nanoparticle-based nanofluids in enhanced oil recovery, Fuel 267 (2020) 117262.
[15] E. Joonaki, S. Ghanaatian, The application of nanofluids for enhanced oil recovery: effects on interfacial tension and coreflooding process, Pet. Sci. Technol. 32 (21) (2014) 2599–2607.
[16] D. Kumar, et al., A review on application of nanoparticles in cEOR: Performance, mechanisms, and influencing parameters, J. Mol. Liq. 353 (2022) 118821.
[17] M. Iravani, Z. Khalilnezhad, A. Khalilnezhad, A review on application of nanoparticles for EOR purposes: history and current challenges, J. Pet. Explor. Prod. Technol. 13 (4) (2023) 959–994.
[18] X. Sun, et al., Application of nanoparticles in enhanced oil recovery: a critical review of recent progress, Energies 10 (3) (2017) 345.
[19] D.T. Wasan, A.D. Nikolov, Spreading of nanofluids on solids, Nature 423 (6936) (2003) 156–159.
[20] K. Kondiparty, et al., Wetting and spreading of nanofluids on solid surfaces driven by the structural disjoining pressure: statics analysis and experiments, Langmuir 27 (7) (2011) 3324–3335.
[21] P. McElfresh, D. Holcomb, D. Ector, Application of nanofluid technology to improve recovery in oil and gas wells. SPE International Oilfield Nanotechnology Conference and Exhibition, SPE, 2012.
[22] D. Arab, A. Kantzas, S.L. Bryant, Nanoparticle stabilized oil in water emulsions: A critical review, J. Pet. Sci. Eng. 163 (2018) 217–242.
[23] A.M. Salem Ragab, A.E. Hannora, A Comparative investigation of nano particle effects for improved oil recovery–experimental work. SPE Kuwait Oil and Gas Show and Conference, SPE, 2015.
[24] A. Karimi, et al., Wettability alteration in carbonates using zirconium oxide nanofluids: EOR implications, Energy & Fuel 26 (2) (2012) 1028–1036.
[25] G. Kumar, et al., Engineering the wettability alteration of sandstone using surfactant-assisted functional silica nanofluids in low-salinity seawater for enhanced oil recovery, ACS Engineering Au 2 (5) (2022) 421–435.
[26] B. Ju, T. Fan, Experimental study and mathematical model of nanoparticle transport in porous media, Powder Technol. 192 (2) (2009) 195–202.
[27] L. Hendraningrat, O. Torsæter, Understanding fluid-fluid and fluid-rock interactions in the presence of hydrophilic nanoparticles at various conditions. SPE Asia Pacific Oil and Gas Conference and Exhibition, SPE, 2014.
[28] L. Hendraningrat, S. Li, O. Torsæter, Effect of some parameters influencing enhanced oil recovery process using silica nanoparticles: an experimental investigation, SPE Reservoir Characterisation and Simulation Conference and Exhibition, SPE, SPE-165955-MS, 2013.
[29] J. Foroozesh, S. Kumar, Nanoparticles behaviors in porous media: Application to enhanced oil recovery, J. Mol. Liq. 316 (2020) 113876.
[30] Y. Sun, et al., Properties of nanofluids and their applications in enhanced oil recovery: a comprehensive review, Energy & Fuel 34 (2) (2020) 1202–1218.
[31] M.N. Agista, K. Guo, Z. Yu, A state-of-the-art review of nanoparticles application in petroleum with a focus on enhanced oil recovery, Appl. Sci. 8 (6) (2018) 871.
[32] N. Chegenizadeh, A. Saeedi, Q. Xie, Application of nanotechnology for enhancing oil recovery–A review, Petroleum 2 (4) (2016) 324–333.
[33] Miranda, C.R., L.S. de Lara, and B.C. Tonetto. Stability and mobility of functionalized silica nanoparticles for enhanced oil recovery applications. in SPE international oilfield nanotechnology conference and exhibition. 2012. SPE.
[34] M.I. Youssif, et al., Silica nanofluid flooding for enhanced oil recovery in sandstone rocks, Egypt. J. Pet. 27 (1) (2018) 105–110.
[35] M.M. Abomughaid, Bio-fabrication of bio-inspired silica nanomaterials from orange peels in combating oxidative stress, Nanomaterials 12 (18) (2022) 3236.
[36] J.H. Luo, et al., A facial route for preparation of hydrophobic nano-silica modified by silane coupling agents, Key Eng. Mater. 727 (2017) 353–358.
[37] A. Bila, J.Å. Stensen, O. Torsæter, Experimental investigation of polymer-coated silica nanoparticles for enhanced oil recovery, Nanomaterials 9 (6) (2019) 822.
[38] M.A. Haruna, et al., Nanoparticle modified polyacrylamide for enhanced oil recovery at harsh conditions, Fuel 268 (2020) 117186.
[39] C. Dai, et al., Spontaneous imbibition investigation of self-dispersing silica nanofluids for enhanced oil recovery in low-permeability cores, Energy & Fuel 31 (3) (2017) 2663–2668.
[40] F. Sagala, A. Hethnawi, N.N. Nassar, Integrating silicate-based nanoparticles with low-salinity water flooding for enhanced oil recovery in sandstone reservoirs, Ind. Eng. Chem. Res. 59 (37) (2020) 16225–16239.
[41] F. Sagala, et al., Nanopyroxene-based nanofluids for enhanced oil recovery in sandstone cores at reservoir temperature, Energy & Fuel 33 (2) (2019) 877–890.
[42] A. Hethnawi, N.N. Nassar, G. Vitale, Preparation and characterization of polyethylenimine-functionalized pyroxene nanoparticles and its application in wastewater treatment, Colloids Surf. A Physicochem. Eng. Asp. 525 (2017) 20–30.
[43] A. Esfandyari Bayat, et al., Transport and retention of engineered Al2O3, TiO2 and SiO2 nanoparticles through various sedimentary rocks, Sci. Rep. 5 (1) (2015) 14264.
[44] Hendraningrat, L., S. Li, and O. Torsaeter. *Enhancing oil recovery of low-permeability Berea sandstone through optimized nanofluids concentration*. in *SPE Asia Pacific Enhanced Oil Recovery Conference*. 2013. SPE.
[45] F. Sagala, et al., Formulation of Spontaneous In Situ Emulsification Using Sodium Lauryl Sulfate Grafted Nanopyroxene for Enhanced Heavy Oil Recovery in Sandstone Reservoirs, Energy & Fuel 37 (17) (2023) 12838–12853.
[46] F. Salem, T. Thiemann, Produced water from oil and gas exploration—problems, solutions and opportunities, J. Water Resour. Prot. 14 (2) (2022) 142–185.
[47] F. Al Salem, T. Thiemann, Variability in Quantity and Salinity of Produced Water from an Oil Production in South Kuwait, Engineering 16 (1) (2024) 8–23.
[48] D.C. Standnes, T. Austad, Wettability alteration in chalk: 1. Preparation of core material and oil properties, J. Pet. Sci. Eng. 28 (3) (2000) 111–121.
[49] H.M. Hegab, et al., Effective in-situ chemical surface modification of forward osmosis membranes with polydopamine-induced graphene oxide for biofouling mitigation, Desalination 385 (2016) 126–137.
[50] M. Shouxiang, N.R. Morrow, X. Zhang, Generalized scaling of spontaneous imbibition data for strongly water-wet systems, J. Pet. Sci. Eng. 18 (3–4) (1997) 165–178.
[51] M. Zhao, et al., Study on the main factors and mechanism of functional silica nanofluid spontaneous imbibition for enhanced oil recovery, J. Mol. Liq. 394 (2024) 123699.
[52] M.A. Haruna, et al., Improved Polymer Flooding in Harsh Environments by Free-Radical Polymerization and the Use of Nanomaterials, Energy & Fuel 33 (2) (2019) 1637–1648.
[53] S.K. Choi, et al., Nanofluid enhanced oil recovery using hydrophobically associative zwitterionic polymer-coated silica nanoparticles, Energy & Fuel 31 (8) (2017) 7777–7782.
[54] G. Jia, et al., Novel zwitterionic-polymer-coated silica nanoparticles, Langmuir 25 (5) (2009) 3196–3199.
[55] M. Khalfaoui, et al., New theoretical expressions for the five adsorption type isotherms classified by BET based on statistical physics treatment, J. Colloid Interface Sci. 263 (2) (2003) 350–356.
[56] S.C. Feifel, F. Lisdat, Silica nanoparticles for the layer-by-layer assembly of fully electro-active cytochrome c multilayers, J. Nanobiotechnol. 9 (1) (2011) 1–12.
[57] Guide, S.D.U., *Online*. Sigma-Aldrich. https://www. sigmaaldrich. com/content/dam/sigmaaldrich/docs/Aldrich/Bulletin/al_exp_guide_pdencat. pdf (accessed October 2018), 2011. **310**.
[58] Z. Hu, et al., Rheological properties of partially hydrolyzed polyacrylamide seeded by nanoparticles, Ind. Eng. Chem. Res. 56 (12) (2017) 3456–3463.
[59] Z. Xu, et al., Oleylamine as both reducing agent and stabilizer in a facile synthesis of magnetite nanoparticles, Chem. Mater. 21 (9) (2009) 1778–1780.
[60] X. Xi, A. Pizzi, L. Delmotte, Isocyanate-free polyurethane coatings and adhesives from mono-and di-saccharides, Polymers 10 (4) (2018) 402.
[61] J. Fang, et al., Needleless melt-electrospinning of polypropylene nanofibres, J. Nanomater. 2012 (2012) 1–9.

[62] Clementz, D.M. Alteration of rock properties by adsorption of petroleum heavy ends: implications for enhanced oil recovery. in SPE Enhanced Oil Recovery Symposium. 1982. OnePetro.
[63] Cuiec, L. Rock/crude-oil interactions and wettability: An attempt to understand their interrelation. in SPE annual technical conference and exhibition. 1984. OnePetro.
[64] J.S. Buckley, C. Bousseau, Y. Liu, Wetting alteration by brine and crude oil: from contact angles to cores, SPE J. 1 (03) (1996) 341–350.
[65] B. Brissault, et al., Synthesis of linear polyethylenimine derivatives for DNA transfection, Bioconjug. Chem. 14 (3) (2003) 581–587.
[66] F. Ahangaran, A.H. Navarchian, Recent advances in chemical surface modification of metal oxide nanoparticles with silane coupling agents: A review, Adv. Colloid Interface Sci. 286 (2020) 102298.
[67] S. Ncube, et al., Recent advances in the adsorbents for isolation of polycyclic aromatic hydrocarbons (PAHs) from environmental sample solutions, TrAC Trends Anal. Chem. 99 (2018) 101–116.
[68] G. Midekessa, et al., Zeta potential of extracellular vesicles: toward understanding the attributes that determine colloidal stability, ACS Omega 5 (27) (2020) 16701–16710.
[69] M.D. Jackson, D. Al-Mahrouqi, J. Vinogradov, Zeta potential in oil-water-carbonate systems and its impact on oil recovery during controlled salinity water-flooding, Sci. Rep. 6 (1) (2016) 37363.
[70] Y. Kazemzadeh, et al., Review on application of nanoparticles for EOR purposes: A critical review of the opportunities and challenges, Chinese Journal of Chemical Engineering 27 (2) (2019) 237–246.
[71] I. Chowdhury, et al., Mechanisms of TiO2 nanoparticle transport in porous media: Role of solution chemistry, nanoparticle concentration, and flowrate, J. Colloid Interface Sci. 360 (2) (2011) 548–555.
[72] E. Nourafkan, et al., Nanoparticle formation in stable microemulsions for enhanced oil recovery application, Ind. Eng. Chem. Res. 58 (28) (2019) 12664–12677.
[73] A.S. Bakshi, R.P. Singh, Kinetics of water diffusion and starch gelatinization during rice parboiling, J. Food Sci. 45 (5) (1980) 1387–1392.
[74] A. Hamza, I.A. Hussein, M. Mahmoud, Introduction to reservoir fluids and rock properties, in: Developments in Petroleum Science, Elsevier, 2023, pp. 1–19.
[75] L.-H. Zhang, et al., Effect of temperature on the oil–water relative permeability for sandstone reservoirs, Int. J. Heat Mass Transf. 105 (2017) 535–548.
[76] W. Anderson, Wettability literature survey-part 2: Wettability measurement, J. Petrol. Tech. 38 (11) (1986) 1246–1262.
[77] U.S. Behera, J.S. Sangwai, Nanofluids of kaolinite and silica in low saline seawater (lowsal) with and without surfactant: interfacial tension and wettability alteration of oil–water–rock system for low salinity-enhanced oil recovery, Ind. Eng. Chem. Res. 60 (1) (2020) 291–313.